

Optical MIMO Multi-mode Fiber Transmission using Photonic Lanterns

Andreas Ahrens, André Sandmann and Steffen Lochmann
*Hochschule Wismar, University of Applied Sciences: Technology, Business and Design,
Philipp-Müller-Straße 14, 23966 Wismar, Germany*

Keywords: Multiple-input Multiple-output Transmission, Optical MIMO, Photonic Lantern, Singular-value Decomposition.

Abstract: Within the last years the multiple-input multiple-output (MIMO) technology has attracted increasing interest in the optical fiber community. Theoretically, the concept of MIMO is well-understood and shows some similarities to wireless MIMO systems. However, practical implementations of optical components are in the focus of interest. Optical couplers have long been used as passive optical components being able to combine or split single-input single-output (SISO) data transmissions. They have been proven to be well-suited for the optical MIMO transmission despite their insertion losses and asymmetries. Nowadays, next to optical couplers, photonic lanterns (PLs) have attracted a lot of attention in the research community as they offer the benefit of a low loss transition from the input fibers to the modes supported by the waveguide at its output. In this contribution the properties of a six-port PL are evaluated by measurements with regards to their respective MIMO suitability. Based on the obtained results, a simplified time-domain MIMO simulation model, including PLs for mode combining at the transmitter-side as well as for mode splitting at the receiver-side, is elaborated. Our results obtained by the simulated bit-error rate (BER) performance as well as by measurements show that PLs are well-suited for the optical MIMO transmission.

1 INTRODUCTION

The growing demand of bandwidth particularly driven by the developing Internet has been satisfied so far by optical fiber technologies such as dense wavelength division multiplexing, polarization division multiplexing and multi-level modulation. These technologies have now reached a state of maturity (Winzer, 2012). The only way to further increase the available data rate is now be seen in the area of spatial multiplexing (Richardson et al., 2013), which is well-established in wireless communications (Tse and Viswanath, 2005). Nowadays several novel techniques such as mode group division multiplexing or multiple-input multiple-output (MIMO) are in the focus of interest (Singer et al., 2008). Among these techniques, the concept of MIMO transmission over multi-mode fibers has attracted increasing interest in the optical fiber transmission community, targeting at increased fiber capacity (Foschini, 1996; Singer et al., 2008; Winzer and Foschini, 2014). The fiber capacity of a multi-mode fiber is limited by the modal dispersion compared to single-mode transmission where no modal dispersion except for polarization exists. In theory, the optical MIMO concept is well-described

(Singer et al., 2008). However, the practical realization of the optical MIMO channel requires substantial further research regarding mode combining, mode maintenance and mode splitting (Schöllmann and Rosenkranz, 2007; Schöllmann et al., 2008; Sandmann et al., 2016; Sandmann et al., 2014). Hence, photonic lanterns (PLs) have attracted a lot of attention in the research community (Leon-Saval et al., 2014). Compared to other passive devices used for mode combining and mode splitting such as optical couplers, PLs offer the benefit of a low loss transition from the input fibers to the modes supported by the waveguide at its output which makes such devices very attractive for optical MIMO communication.

Against this background, the novel contribution of this paper is that based on measurements the suitability of PLs for mode combining and splitting is studied by computer simulations.

The remaining parts of this paper are structured as follows: Section 2 introduces the studied optical MIMO system based on PLs and shows measured characteristics of a 6-port PL. Based on these characteristics in section 3 a corresponding electrical MIMO channel model is derived. The block-oriented and SVD-based broadband MIMO system is described in

section 4. The associated performance results are presented and interpreted in section 5. Finally, section 6 provides the concluding remarks.

2 OPTICAL MIMO TRANSMISSION

One approach to form an optical MIMO system is to transmit multiple data signals on different spatial modes through a few-mode or multi-mode fiber (FMF/ MMF). In this work, photonic lanterns (PLs) are studied in order to transfer the binary information carried on the LP_{01} mode in n_T single-mode fibers (SMFs) to discrete modes in a FMF and vice versa. The physical transmission model is depicted in Fig. 1. The FMF carries n_M modes depending on the geometric as well as the physical structure of the fiber and the operating wavelength. Subsequent to the transmission through a FMF of length ℓ , the modes are demultiplexed to n_R SMFs with an inversely arranged PL.

In theory, for transitioning the incident modes of the SMF to the respective modes carried in the few mode fiber with low loss the condition $n_T = n_M = n_R$ needs to be respected (Leon-Saval et al., 2013). However, measurements of the transfer characteristic of the fusion type PL with 6-ports shows quite a noticeable insertion loss and slight asymmetries between the different SMF inputs, see Tab. 1. Still, these asymmetries are relatively small when comparing to the insertion loss differences of an optical MIMO system based on offset SMF to MMF splices and fusion couplers as shown in the same table (Sandmann et al., 2016). Contrary to expectations, the photonic integrated circuit (PIC) type 6-port PL shows the best results with respect to the insertion loss. Extending a fusion coupler based system to 6-ports requires the concatenation of multiple 2-port systems which is accompanied by a significant insertion loss increase.

Considering the modal behavior, under ideal conditions the PL transfers the signals from each SMF to a discrete mode in the FMF, see Fig. 2. In contrast, three spatial intensity patterns measured at the output of the 6-port PL, compare Fig. 3, show that a real PL excites a combination of modes which are super-

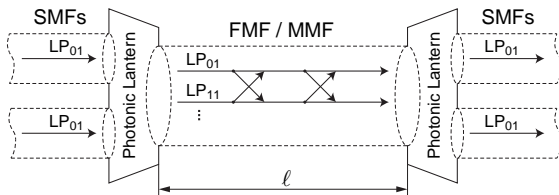


Figure 1: Multi-mode MIMO transmission model using photonic lanterns for mode combining and splitting.

imposed in the FMF, e.g. the LP_{01} and LP_{11} modes. This can be interpreted as cross-talk. In addition to the cross-talk introduced by the PLs, mode mixing during the transmission through the FMF occurs due to micro bends etc. The idea is to apply MIMO signal processing in order to remove the cross-talk. For this purpose, the transmission relations are described in an electrical system model.

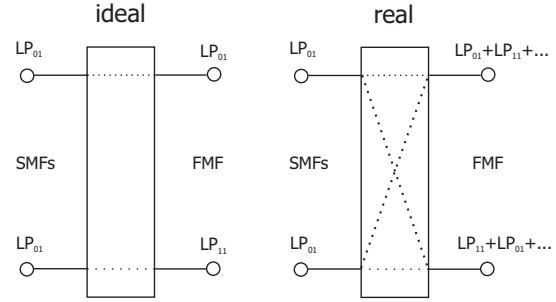


Figure 2: Comparing the spatial mode transformation characteristic of a real PL with an ideal PL.

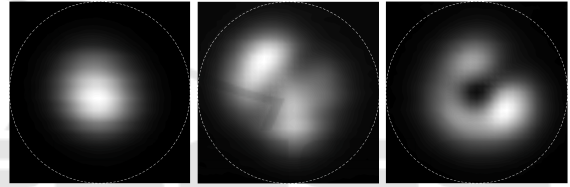


Figure 3: Example of measured spatial intensity patterns at the output of a fusion type PL using different input SMFs at an operating wavelength of $\lambda = 1550$ nm; the dotted line represents the $30 \mu\text{m}$ fiber core diameter.

3 ELECTRICAL MIMO CHANNEL REPRESENTATION

The electrical baseband MIMO channel representation employing PLs and a FMF is shown in Fig. 4. Here, the transmitter-side photonic lantern is fed by the signals $a_\mu(t)$, with $\mu = 1, \dots, n_T$, representing the optical signals carried on the LP_{01} mode in the SMFs. Correspondingly, the signals $b_\beta(t)$ represent the guided spatial modes at the input of the FMF and $c_\kappa(t)$ are the resulting FMF output signals, where

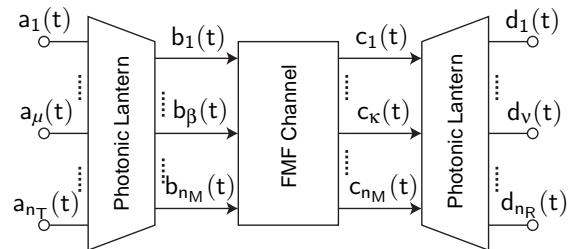


Figure 4: Electrical MIMO channel model.

Table 1: Insertion loss measurements when launching from different SMF inputs through a fusion type and photonic integrated circuit (PIC) type 6-port photonic lantern compared to a 2-port fusion coupler based system.

SMF input number	1	2	3	4	5	6
Fusion type PL insert. loss [dB]	6.7	6.7	4.2	4.1	7.0	4.1
PIC type PL insert. loss [dB]	1.7	2.2	1.5	2.2	2.0	1.7
Fusion coupler insert. loss [dB]	0.1	8.1	-	-	-	-

$\beta, \kappa = 1, \dots, n_M$. Finally, the receiver-side PL transfers the modes of the FMF to fundamental modes in the SMFs, represented by the signals $d_v(t)$, with $v = 1, \dots, n_R$. For simplification purposes and in order to create the prerequisites for a near lossless transmission the number of input SMFs n_T , the number of guided modes in the FMF n_M and the number of output SMFs n_R are assumed to be identically. In this work, these numbers are chosen to be $n_T = n_M = n_R = 2$ and therefore only the LP_{01} and LP_{11} modes can propagate implying a V-number in range $2.405 < V < 3.832$ when transmitting through a step-index profiled FMF. The degenerate modes of LP_{11} , i.e. LP_{11a} and LP_{11b} , are summarized.

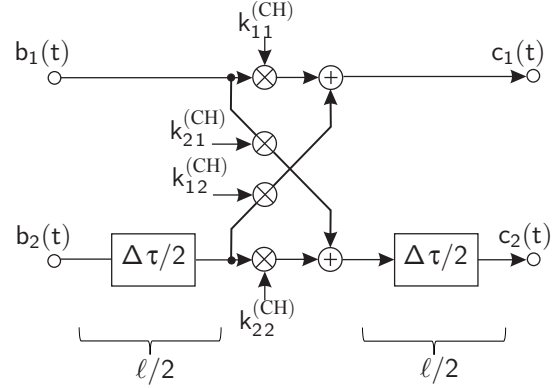
3.1 FMF Channel

The transmission properties of the FMF are represented by the model depicted in Fig. 5. In time-domain, the system characteristics of the FMF channel are given as follows

$$\begin{aligned} c_1(t) &= k_{11}^{(CH)} b_1(t) + k_{12}^{(CH)} b_2(t - \Delta\tau/2) \\ c_2(t) &= k_{21}^{(CH)} b_1(t - \Delta\tau/2) + k_{22}^{(CH)} b_2(t - \Delta\tau) \end{aligned} \quad (1)$$

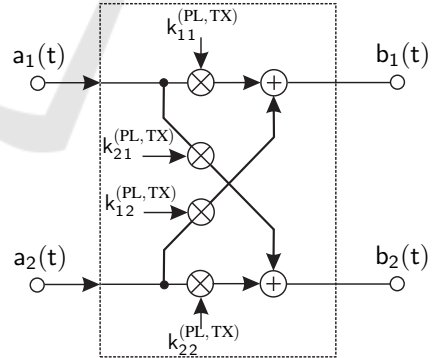
describing the mode-coupling of the underlying channel. Herein, the parameter $\Delta\tau$ describes the differential mode delay between the fundamental mode LP_{01} and the mode LP_{11} , which is identified to be $\Delta\tau = 200$ ps for the considered fiber length of $\ell = 2$ km. The effect of the chromatic dispersion is not analyzed in this contribution since a zero chromatic dispersion wavelength is assumed which is in the region of 1300 nm. However, for different wavelengths chromatic dispersion can be taken into account by a simple convolution with a Gaussian function. The optical field coupling coefficients $k_{\kappa\beta}^{(CH)}$ describe the coupling from the mode LP_{01} to the mode LP_{11} , from the mode LP_{11} to the mode LP_{01} and so forth. Since a lossless transmission through the FMF is assumed, the coupling coefficients have to fulfill the following condition

$$\sum_{\kappa=1}^{n_M} |k_{\kappa\beta}^{(CH)}|^2 = 1 \quad \forall \beta. \quad (2)$$

Figure 5: Underlying FMF channel model of length ℓ designed for two mode propagation ($n_M = 2$).

3.2 Photonic Lanterns

Hereinafter, the mode combining and mode splitting process conducted by the photonic lanterns is studied. Considering a (2×2) PL the corresponding electrical representation for the transmitter-side PL is shown in Fig. 6. At the transmitter-side the mapping of the

Figure 6: Electrical system model of the transmitter-side PL ($n_T = n_M = 2$).

incident LP_{01} modes, represented by the signals $a_\mu(t)$, by the PL can be described with the corresponding coupling matrix

$$\mathbf{K}^{(TX)} = \begin{bmatrix} k_{11}^{(PL,TX)} & \dots & k_{1n_T}^{(PL,TX)} \\ \vdots & \ddots & \vdots \\ k_{n_M 1}^{(PL,TX)} & \dots & k_{n_M n_T}^{(PL,TX)} \end{bmatrix}, \quad (3)$$

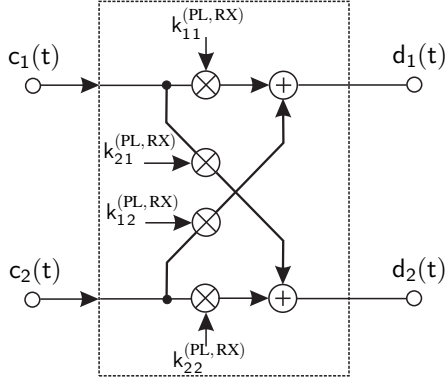


Figure 7: Electrical system model of the receiver-side PL ($n_M = n_R = 2$).

with $k_{\beta\mu}^{(\text{PL,TX})}$ denoting the transmitter-side coupling coefficients. Having an ideal PL, compare Fig. 2, the coupling matrix is given by an identity matrix considering $n_M = n_T$. Since the receiver-side PL is inversely arranged and is assumed to have identical properties to the transmitter-side PL, the corresponding coupling matrix is the transpose denoted by $(\cdot)^T$ of the transmitter-side coupling matrix, i.e. $\mathbf{K}^{(\text{RX})} = (\mathbf{K}^{(\text{TX})})^T$. Here, it is worth noting that under practical assumptions the output LP_{01} modes of the receiver-side PL appear as superpositions of the LP_{01} and LP_{11} modes of the FMF as highlighted in Fig. 2. Having a non-ideal PL, the corresponding electrical system model is shown in Fig. 7 for the receiver-side PL. Here, $k_{\nu\kappa}^{(\text{PL,RX})}$ denotes the receiver-side coupling coefficients, being summarized in the coupling matrix $\mathbf{K}^{(\text{RX})}$. Based on the short fiber length, the PL is assumed to be flat in the considered frequency band. Since no power-loss is assumed, the transmitter-side PL coupling coefficients are required to comply to

$$\sum_{\beta=1}^{n_M} |k_{\beta\mu}^{(\text{PL,TX})}|^2 = 1 \quad \text{for } \mu = 1, \dots, n_T \quad (4)$$

and the receiver-side PL coupling coefficients need to fulfill the following condition

$$\sum_{\nu=1}^{n_R} |k_{\nu\kappa}^{(\text{PL,RX})}|^2 = 1 \quad \text{for } \kappa = 1, \dots, n_M \quad (5)$$

Considering the overall MIMO channel model, compare Fig. 4, as a black box with two in- and outputs the transfer characteristic can be described by the corresponding MIMO impulse responses $g_{\nu\mu}(t)$. Including pulse shaping and receive filtering functionality the overall (2×2) MIMO transmission model is depicted in Fig. 8. Rectangular pulses of frequency

$f_T = 1/T_s$ are used for pulse shaping and receive filtering, i.e. $g_s(t)$ and $g_{\text{ef}}(t)$ and hence the overall impulse responses $h_{\nu\mu}(t)$ are formed as follows

$$h_{\nu\mu}(t) = g_s(t) * g_{\nu\mu}(t) * g_{\text{ef}}(t) \quad , \quad (6)$$

where $*$ denotes the convolution operator. An additional component to be considered is the additive white Gaussian noise (AWGN) denoted by the term $\tilde{n}_v(t)$. The sampled overall impulse responses are used for the broadband MIMO system model, being described in the next section.

4 BROADBAND MIMO SYSTEM DESCRIPTION

Considering a frequency-selective MIMO link, composed of n_T optical inputs and n_R optical outputs, the resulting electrical discrete-time block-oriented system is modeled referring to (Raleigh and Cioffi, 1998; Pankow et al., 2011) as follows

$$\mathbf{u} = \mathbf{H} \cdot \mathbf{b} + \mathbf{n} \quad . \quad (7)$$

Vector \mathbf{b} of size $(N_T \times 1)$ contains the input symbols transmitted over n_T optical inputs in K consecutive time slots, i.e. $N_T = K n_T$. This vector can be decomposed into n_T input-specific signal vectors \mathbf{b}_μ according to

$$\mathbf{b} = [\mathbf{b}_1^T, \dots, \mathbf{b}_\mu^T, \dots, \mathbf{b}_{n_T}^T]^T \quad , \quad (8)$$

where $(\cdot)^T$ denotes the transpose operator. These input-specific signal vectors of size $(K \times 1)$ include the symbols transmitted at the optical input μ for all time instances k , with $k = 1, \dots, K$, as given by

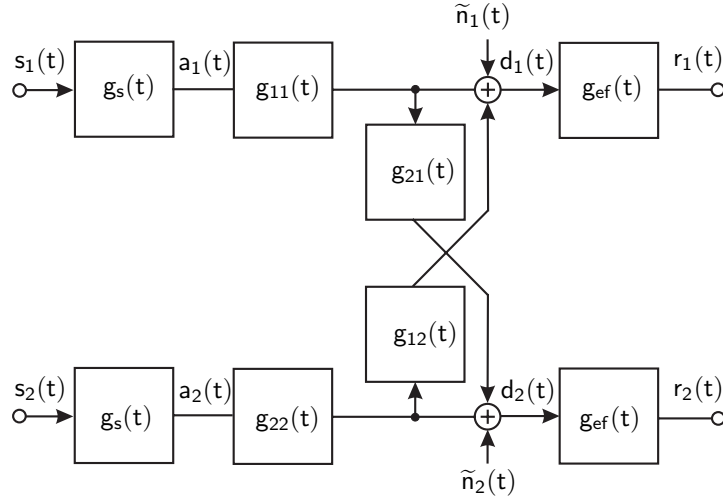
$$\mathbf{b}_\mu = [b_{1\mu}, \dots, b_{k\mu}, \dots, b_{K\mu}]^T \quad . \quad (9)$$

The $(N_R \times 1)$ sized received signal vector \mathbf{u} can again be decomposed into n_R output-specific signal vectors \mathbf{u}_ν of the length $K + L_c$, i.e. $N_R = (K + L_c) n_R$, and results in

$$\mathbf{u} = [\mathbf{u}_1^T, \dots, \mathbf{u}_\nu^T, \dots, \mathbf{u}_{n_R}^T]^T \quad . \quad (10)$$

By taking the $(L_c + 1)$ non-zero elements of the resulting symbol rate sampled overall channel impulse response $h_{\nu\mu}(t)$ between the μ th input and ν th output into account, the output-specific received vector \mathbf{u}_ν has to be extended by L_c elements, compared to the transmitted input-specific signal vector \mathbf{b}_μ defined in (9). The $((K + L_c) \times 1)$ signal vector \mathbf{u}_ν received by the optical output ν can be constructed, including the extension through the multi-path propagation, as follows

$$\mathbf{u}_\nu = [u_{1\nu}, u_{2\nu}, \dots, u_{(K+L_c)\nu}]^T \quad . \quad (11)$$


 Figure 8: Electrical (2×2) MIMO transmission model.

Correspondingly, the $(N_R \times 1)$ sized vector \mathbf{n} denotes the AWGN after receive filtering with $g_{ef}(t)$ and sampling. Finally, the $(N_R \times N_T)$ sized system matrix \mathbf{H} of the block-oriented system model describes the symbol rate sampled overall MIMO channel $h_{\nu\mu}(t)$ consisting of the frequency-flat transmitter- and receiver-side PL models as well as the frequency-selective FMF model, the transmit and receive filter. The channel matrix \mathbf{H} is composed as follows

$$\mathbf{H} = \mathbf{H}^{(RX)} \cdot \mathbf{H}^{(CH)} \cdot \mathbf{H}^{(TX)}. \quad (12)$$

Herein, the $(n_M(K + L_c) \times n_M K)$ sized matrix $\mathbf{H}^{(CH)}$ describes the frequency-selective representation of the FMF channel, compare Fig. 5, being structured as follows

$$\mathbf{H}^{(CH)} = \begin{bmatrix} \mathbf{H}_{11}^{(CH)} & \cdots & \mathbf{H}_{1n_M}^{(CH)} \\ \vdots & \ddots & \vdots \\ \mathbf{H}_{n_M 1}^{(CH)} & \cdots & \mathbf{H}_{n_M n_M}^{(CH)} \end{bmatrix} \quad (13)$$

and consists of $n_M n_M$ single-input single-output (SISO) channel matrices $\mathbf{H}_{\kappa\beta}^{(CH)}$. Every of these matrices $\mathbf{H}_{\kappa\beta}^{(CH)}$ of the size $((K + L_c) \times K)$ describes the $L_c + 1$ non-zero elements of resulting symbol rate sampled impulse response of the FMF channel representation including transmit and receive filtering, resulting in:

$$\mathbf{H}_{\kappa\beta}^{(CH)} = \begin{bmatrix} h_{\kappa\beta}[0] & 0 & \cdots & 0 \\ h_{\kappa\beta}[1] & h_{\kappa\beta}[0] & \cdots & 0 \\ h_{\kappa\beta}[2] & h_{\kappa\beta}[1] & \cdots & 0 \\ \vdots & \vdots & \ddots & \vdots \\ h_{\kappa\beta}[L_c] & h_{\kappa\beta}[L_c - 1] & \cdots & \vdots \\ 0 & h_{\kappa\beta}[L_c] & \cdots & \vdots \\ \vdots & \vdots & \ddots & \vdots \\ 0 & 0 & \cdots & h_{\kappa\beta}[L_c] \end{bmatrix}. \quad (14)$$

Since the transmitter-side photonic lantern (PL) is assumed to be frequency-flat it can be described by a $((n_M K) \times (n_T K))$ pre-processing matrix

$$\mathbf{H}^{(TX)} = \mathbf{K}^{(TX)} \otimes \mathbf{I}_K, \quad (15)$$

where \otimes denotes the Kronecker product, $\mathbf{K}^{(TX)}$ is the transmitter-side PL coupling matrix and \mathbf{I}_K defines a $(K \times K)$ identity matrix. Matrix $\mathbf{H}^{(TX)}$ is composed of concatenated $(K \times K)$ sized diagonal matrices weighted by the corresponding coupling factors $k_{\beta\mu}^{(PL, TX)}$. Correspondingly the receiver-side PL can be described by a $(n_R(K + L_c) \times n_M(K + L_c))$ post-processing matrix

$$\mathbf{H}^{(RX)} = \mathbf{K}^{(RX)} \otimes \mathbf{I}_{K+L_c}, \quad (16)$$

with $\mathbf{K}^{(RX)}$ denoting the receiver-side PL coupling matrix. The interference, which is introduced by the off-diagonal elements of the channel matrix \mathbf{H} , requires appropriate signal processing strategies.

The MIMO block diagram of the transmission model is shown in Fig. 9. A popular technique is based on the singular-value decomposition (SVD) of the system matrix \mathbf{H} , which can be written as

$$\mathbf{H} = \mathbf{S} \cdot \mathbf{V} \cdot \mathbf{D}^H, \quad (17)$$

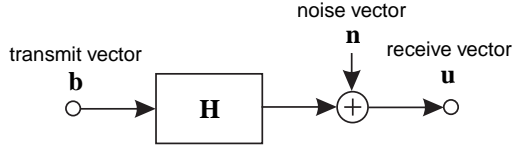


Figure 9: Transmission system model.

where \mathbf{S} and \mathbf{D}^H are unitary matrices and \mathbf{V} is a real-valued diagonal matrix of the positive square roots of the eigenvalues of the matrix $\mathbf{H}^H \mathbf{H}$ sorted in descending order. In order to remove the interferences pre-processed symbols $\mathbf{b} = \mathbf{D} \cdot \mathbf{c}$ are transmitted, with vector \mathbf{c} denoting the unprocessed transmit symbols. In turn, the receiver multiplies the received vector \mathbf{u} by the matrix \mathbf{S}^H . Thereby, neither the transmit power nor the noise power is enhanced. The overall transmission relationship is defined as

$$\mathbf{y} = \mathbf{S}^H (\mathbf{H} \cdot \mathbf{D} \cdot \mathbf{c} + \mathbf{n}) = \mathbf{V} \cdot \mathbf{c} + \mathbf{w}. \quad (18)$$

As a consequence of the processing in (18), the channel matrix \mathbf{H} is transformed into independent, non-interfering layers having unequal gains (Pankow et al., 2011; Raleigh and Cioffi, 1998; Ahrens and Benavente-Peces, 2009). In MIMO communication, singular-value decomposition (SVD) has been established as an efficient concept to compensate the interferences between the different data streams transmitted over a dispersive channel: SVD is able to transfer the whole system into independent, non-interfering layers exhibiting unequal gains per layer as highlighted in Fig. 10, where as a result weighted AWGN channels appear.

Analyzing the considered (2×2) MIMO system, the data symbols at the time k , i.e. c_{1k} and c_{2k} are weighted by the positive square roots of the eigenvalues of the matrix $\mathbf{H}^H \mathbf{H}$, i.e. $\sqrt{\xi_{1k}}$ and $\sqrt{\xi_{2k}}$. The terms w_{1k} and w_{2k} denote the noise subsequent to the SVD post-processing. It is worth noting that the number of readily separable layers is limited by $\min(n_T, n_R)$. Therefore, in this work the maximum number of layers is given by $L = 2$. Based on this non-interfering layer-specific transmission model the bit-error rate performance can be calculated (Proakis, 2000).

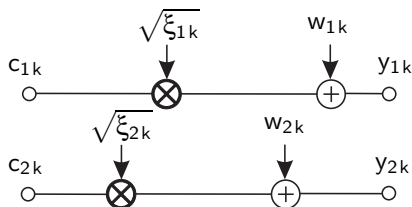


Figure 10: SVD-based layer-specific transmission model.

5 PERFORMANCE RESULTS

In this section the BER quality, transmitting through the (2×2) MIMO channel employing PLs for mode combining and splitting, is studied using fixed transmission modes with a spectral efficiency of 4 bit/s/Hz. The analyzed quadrature amplitude modulation (QAM) constellations are listed in Tab. 2. This

Table 2: Transmission modes.

Spectral Efficiency	Layer 1	Layer 2
4 bit/s/Hz	16	0
4 bit/s/Hz	4	4

bit allocation approach is combined with a power allocation method that equalizes the signal-to-noise ratios on all layers and time instances k in a data block for optimizing the BER performance (Sandmann et al., 2015).

In order to compare the performance of ideal PLs to real PLs different cross-talk parameters have been considered relating to the above described electrical MIMO channel model. Since both PLs are assumed to have identical properties in both directions and are also assumed to be symmetric the PL cross-talk parameter is defined as follows

$$\begin{aligned} p_{\text{cross}}^{(\text{PL})} &= |k_{12}^{(\text{PL},\text{TX})}|^2 = |k_{21}^{(\text{PL},\text{TX})}|^2 \\ &= |k_{12}^{(\text{PL},\text{RX})}|^2 = |k_{21}^{(\text{PL},\text{RX})}|^2, \end{aligned} \quad (19)$$

describing the electrical power transfer. The few-mode fiber channel cross-talk is assumed to be symmetric as well as defined by

$$p_{\text{cross}}^{(\text{CH})} = |k_{12}^{(\text{CH})}|^2 = |k_{21}^{(\text{CH})}|^2. \quad (20)$$

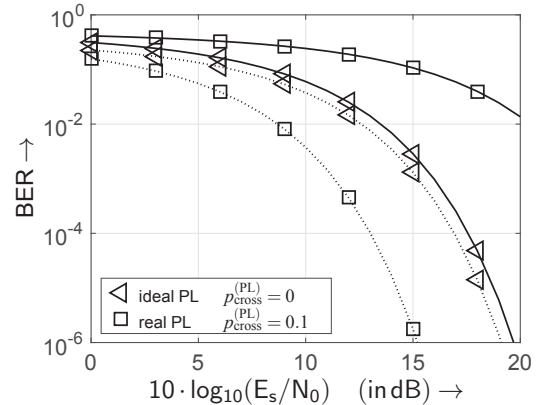


Figure 11: BER performance when transmitting with the $(16,0)$ QAM constellation (dotted lines) and the $(4,4)$ QAM constellation (solid lines) assuming 10% FMF cross-talk, i.e. $p_{\text{cross}}^{(\text{CH})} = 0.1$, at a symbol frequency of $f_T = 1$ GHz.

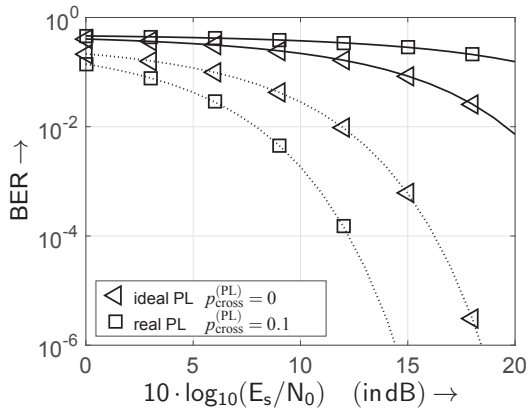


Figure 12: BER performance when transmitting with the (16,0) QAM constellation (dotted lines) and the (4,4) QAM constellation (solid lines) assuming 30% FMF cross-talk, i.e. $p_{\text{cross}}^{(\text{CH})} = 0.3$, at a symbol frequency of $f_T = 1$ GHz.

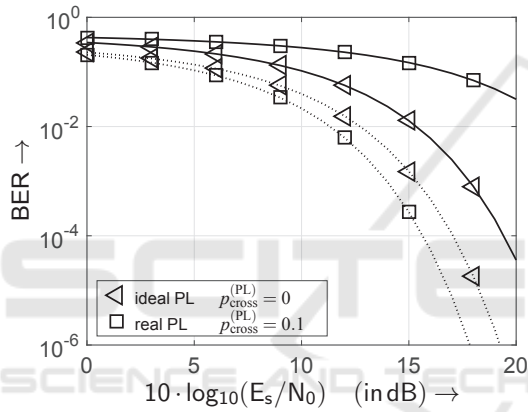


Figure 13: BER performance when transmitting with the (16,0) QAM constellation (dotted lines) and the (4,4) QAM constellation (solid lines) assuming 30% FMF cross-talk, i.e. $p_{\text{cross}}^{(\text{CH})} = 0.3$, at a symbol frequency of $f_T = 5$ GHz.

The calculated BER results as a function of the signal energy to noise power spectral density E_s/N_0 are depicted in Fig. 11, 12 and 13 for different FMF cross-talk parameter choices, i.e. $p_{\text{cross}}^{(\text{CH})}$, and symbol frequencies f_T . In all simulations the number of symbols per data block and per layer is selected to be $K = 15$. Choosing the (16,0) QAM constellation shows the best BER performance results for all configurations considering a real PL. The additional cross-talk introduced by a real PL increases the MIMO channel correlation and thus the amplitude ratio comparing the singular values of the two layers increases as well. Therefore, the (16,0) QAM scheme benefits from the additional cross-talk. In contrast, the increased asymmetry of singular values impairs the BER performance choosing the (4,4) QAM constellation as highlighted by the results.

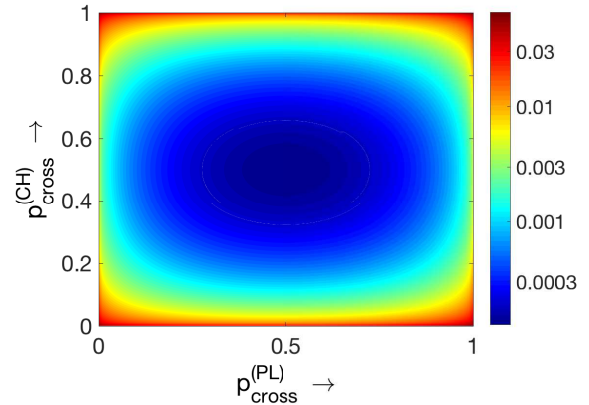


Figure 14: BER performance comparing different cross-talk parameter choices when transmitting with the (16,0) QAM constellation at a fixed E_s/N_0 ratio of 10 dB at a symbol frequency of $f_T = 1$ GHz.

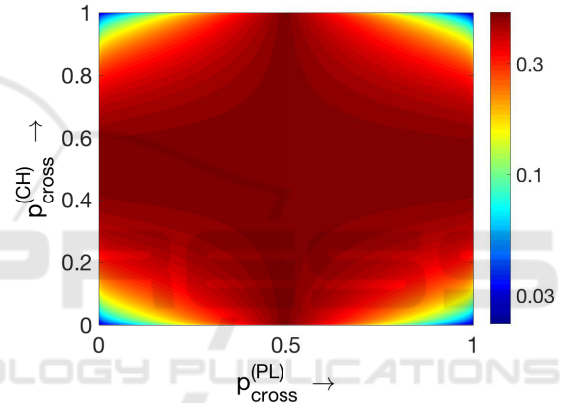


Figure 15: BER performance comparing different cross-talk parameter choices when transmitting with the (4,4) QAM constellation at a fixed E_s/N_0 ratio of 10 dB at a symbol frequency of $f_T = 1$ GHz.

A second study shows the achieved BERs comparing different cross-talk parameter choices, i.e. $p_{\text{cross}}^{(\text{CH})}$ and $p_{\text{cross}}^{(\text{PL})}$, for the (16,0) QAM constellation in Fig. 14 and for the (4,4) QAM scheme in Fig. 15 at a fixed E_s/N_0 ratio of 10 dB. This study confirms that the (16,0) QAM constellation benefits from high cross-talk values whereas the (4,4) QAM constellation shows a contrary behavior. It should be noted that 0.5 for $p_{\text{cross}}^{(\text{CH})}$ as well as for $p_{\text{cross}}^{(\text{PL})}$ is the value where the most cross-talk is introduced into the system. All in all, the best BER results are achieved with the (16,0) QAM constellation in combination with high cross-talk values when considering the studied simulation environment.

6 CONCLUSIONS

In this contribution photonic lanterns as a mode coupling and splitting device have been analyzed with regard to their respective MIMO suitability. The established time-domain MIMO simulation model has been proven to be a versatile tool for the optimization of the overall MIMO transmission performance. It has been shown that the excitation of different mode combinations by the PL, which has been interpreted as cross-talk, does not impair the transmission quality. In certain constellations this cross-talk can help to increase the BER performance. All in all, PLs seem to be well-suited for optical MIMO communication systems.

ACKNOWLEDGEMENTS

This work has been funded by the German Ministry of Education and Research (No. 03FH016PX3).

REFERENCES

- Ahrens, A. and Benavente-Peces, C. (2009). Modulation-Mode and Power Assignment in Broadband MIMO Systems. *Facta Universitatis (Series Electronics and Energetics)*, 22(3):313–327.
- Foschini, G. J. (1996). Layered Space-Time Architecture for Wireless Communication in a Fading Environment when using Multi-Element Antennas. *Bell Labs Technical Journal*, 1(2):41–59.
- Leon-Saval, S. G., Argyros, A., and Bland-Hawthorn, J. (2013). Photonic lanterns. *Nanophotonics*, 2:429–440.
- Leon-Saval, S. G., Fontaine, N. K., Salazar-Gil, J. R., Er-can, B., Ryf, R., and Bland-Hawthorn, J. (2014). Mode-selective photonic lanterns for space-division multiplexing. *Opt. Express*, 22(1):1036–1044.
- Pankow, J., Aust, S., Lochmann, S., and Ahrens, A. (2011). Modulation-Mode Assignment in SVD-assisted Optical MIMO Multimode Fiber Links. In *15th International Conference on Optical Network Design and Modeling (ONDM)*, Bologna, Italy.
- Proakis, J. G. (2000). *Digital Communications*. McGraw-Hill, Boston.
- Raleigh, G. G. and Cioffi, J. M. (1998). Spatio-Temporal Coding for Wireless Communication. *IEEE Transactions on Communications*, 46(3):357–366.
- Richardson, D. J., Fini, J., and Nelson, L. (2013). Space Division Multiplexing in Optical Fibres. *Nature Photonics*, 7:354–362.
- Sandmann, A., Ahrens, A., and Lochmann, S. (2014). Experimental Description of Multimode MIMO Channels utilizing Optical Couplers. In *Photonic Networks; 15. ITG Symposium; Proceedings of*, pages 1–6.
- Sandmann, A., Ahrens, A., and Lochmann, S. (2015). Power Allocation in PMSVD-based Optical MIMO Systems. In *Advances in Wireless and Optical Communications (RTUWO)*, pages 108–111, Riga (Latvia).
- Sandmann, A., Ahrens, A., and Lochmann, S. (2016). Experimental Evaluation of a (4x4) Multi-Mode MIMO System Utilizing Customized Optical Fusion Couplers. In *ITG-Fachbericht 264: Photonische Netze*, pages 101–105, Leipzig (Germany). VDE VERLAG GmbH.
- Schöllmann, S. and Rosenkranz, W. (2007). Experimental Equalization of Crosstalk in a 2 x 2 MIMO System Based on Mode Group Diversity Multiplexing in MMF Systems @ 10.7 Gb/s. In *Optical Communication (ECOC), 2007 33rd European Conference and Exhibition of*, pages 1–2.
- Schöllmann, S., Schrammar, N., and Rosenkranz, W. (2008). Experimental Realisation of 3 x 3 MIMO System with Mode Group Diversity Multiplexing Limited by Modal Noise. In *Optical Fiber Communication Conference/National Fiber Optic Engineers Conference (OFC/NFOEC)*, pages 1–3.
- Singer, A. C., Shanbhag, N. R., and Bae, H. M. (2008). Electronic Dispersion Compensation - An Overview of Optical Communications Systems. *IEEE Signal Processing Magazine*, 25(6):110–130.
- Tse, D. and Viswanath, P. (2005). *Fundamentals of Wireless Communication*. Cambridge, New York.
- Winzer, P. (2012). Optical Networking beyond WDM. *IEEE Photonics Journal*, 4:647–651.
- Winzer, P. J. and Foschini, G. J. (2014). Optical MIMO-SDM system capacities. In *Optical Fiber Communications Conference and Exhibition (OFC), 2014*, pages 1–3.